



OPEN ACCESS

EDITED BY

Ran Tian,
Tianjin Medical University, China

REVIEWED BY

Qiang Zhang,
Tianjin University of Technology, China
Nuo Yu,
Donghua University, China

*CORRESPONDENCE

Nuernisha Alifu,
nens_xjmu@126.com
Xueliang Zhang,
shuxue2456@126.com

[†]These authors have contributed equally to this work

SPECIALTY SECTION

This article was submitted to Nanobiotechnology, a section of the journal Frontiers in Bioengineering and Biotechnology

RECEIVED 01 July 2022

ACCEPTED 30 August 2022

PUBLISHED 19 September 2022

CITATION

Fan H, Yan T, Chen S, Du Z, Alimu G, Zhu L, Ma R, Tang X, Heng Y, Alifu N and Zhang X (2022), Polydopamine encapsulated new indocyanine green theranostic nanoparticles for enhanced photothermal therapy in cervical cancer HeLa cells.
Front. Bioeng. Biotechnol. 10:984166.
doi: 10.3389/fbioe.2022.984166

COPYRIGHT

© 2022 Fan, Yan, Chen, Du, Alimu, Zhu, Ma, Tang, Heng, Alifu and Zhang. This is an open-access article distributed under the terms of the [Creative Commons Attribution License \(CC BY\)](https://creativecommons.org/licenses/by/4.0/). The use, distribution or reproduction in other forums is permitted, provided the original author(s) and the copyright owner(s) are credited and that the original publication in this journal is cited, in accordance with accepted academic practice. No use, distribution or reproduction is permitted which does not comply with these terms.

Polydopamine encapsulated new indocyanine green theranostic nanoparticles for enhanced photothermal therapy in cervical cancer HeLa cells

Huimin Fan^{1†}, Ting Yan^{2†}, Shuang Chen³, Zhong Du³, Gulinigaer Alimu², Lijun Zhu², Rong Ma³, Xiaohui Tang⁴, Youqiang Heng⁵, Nuernisha Alifu^{1*} and Xueliang Zhang^{1*}

¹State Key Laboratory of Pathogenesis, Prevention and Treatment of High Incidence Diseases in Central Asia, School of Medical Engineering and Technology, Xinjiang Medical University, Urumqi, China, ²Department of Epidemiology and Health Statistics, School of Public Health, Xinjiang Medical University, Urumqi, China, ³State Key Laboratory of Pathogenesis, Prevention and Treatment of High Incidence Diseases in Central Asia, Department of Gynecology, The First Affiliated Hospital of Xinjiang Medical University, Urumqi, China, ⁴Central Laboratory of Xinjiang Medical University, Urumqi, China, ⁵State Key Laboratory of Pathogenesis, Prevention and Treatment of High Incidence Diseases in Central Asia, Urumqi, China

Photothermal therapy (PTT) has attracted extensive attention in cancer treatment due to its non-invasiveness, high efficiency, and repeatability in recent years. Photothermal agents (PTAs) are the key factor for PTT. Recently, although an increasing number of PTAs have been developed, there is still a great demand for optimized photothermal nanoparticles (NPs) with low toxicity, bio-safety and stability. Herein, new indocyanine green (IR820) with near-infrared (NIR:700–1,700 nm) fluorescence emission was selected as a photothermal agent (PTA). To enhance the PTT property, IR820 was encapsulated with another kind of PTA, polydopamine (PDA) under alkaline conditions. Furthermore, to improve the biocompatibility of the NPs, methoxy polyethylene glycol amine (mPEG-NH₂) was modified *via* a Michael addition to form a novel kind of IR820@PDA@PEG NPs. After detailed characterization and analysis, the obtained IR820@PDA@PEG NPs showed a spherical shape with an average diameter of ~159.6 nm. Meanwhile, the formed IR820@PDA@PEG NPs exhibited better photostability and lower cytotoxicity than free IR820 molecules. The photothermal performance of IR820@PDA@PEG NPs was further analyzed *in vitro*, and the temperature of IR820@PDA@PEG NPs (100 µg/ml) reached 54.8°C under 793 nm laser irradiation. Afterwards, the cellular uptake of IR820@PDA@PEG NPs was evaluated *via* confocal laser scanning fluorescence microscopic imaging. Then, PTT experiments on HeLa cells demonstrated that IR820@PDA@PEG NPs can hyperthermal ablate cancer cells (~49.1%) under 793 nm laser irradiation. Therefore, IR820@PDA@PEG NPs would be a promising PTA for the treatment of cervical cancer HeLa cells.

KEYWORDS

cervical cancer, new indocyanine green, polydopamine, photothermal therapy, nanoparticles

Introduction

Although the prevention and diagnosis have made great progress (Schiffman et al., 2016; Enokida et al., 2021; Zhang et al., 2022), cervical cancer is still the second most common malignancy in females around the world (Ginsburg et al., 2017). Traditional cancer treatments such as surgery, chemotherapy and radiotherapy have certain side effects (Cohen et al., 2019; Dong et al., 2019; Lungu et al., 2019). Therefore, there is an urgent need to develop an efficient and safe treatment against cervical cancer.

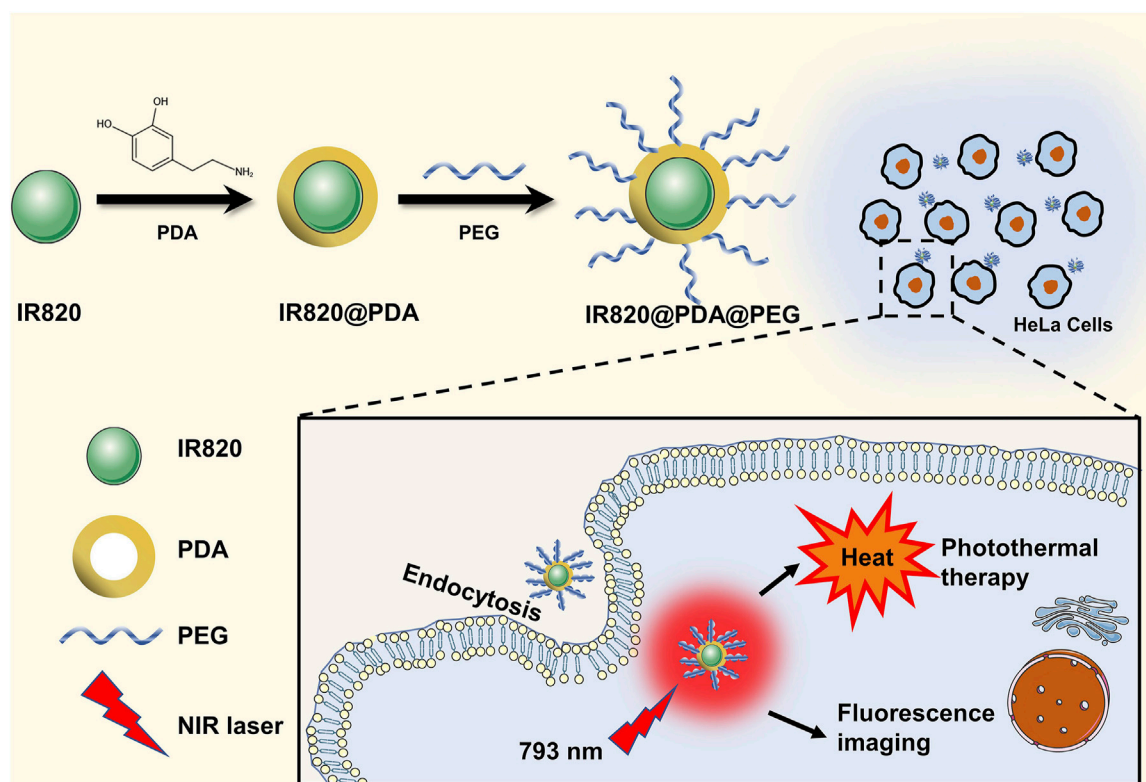
PTT is a favorable strategy for tumor treatment (Nam et al., 2018; Xiao et al., 2021), which induces a local temperature rise to ablate tumors with the assistance of PTAs (Hu et al., 2020; Wang et al., 2021). PTT showed advantages of controllability, minimal invasion, and low side effects in biomedical applications (Li J. et al., 2019; Liu et al., 2020; Ren et al., 2020). It is well known that effective therapeutic effects rely on PTAs with high ability to convert light into heat energy. Until now, a variety of PTAs have been developed successively (Chen et al., 2019), including inorganic PTAs, such as semiconductors (Meng et al., 2016; Yu et al., 2017; Wang et al., 2020a; Wang et al., 2020b), metals (Nuo et al., 2018; Hong et al., 2020), metalloids (Yu et al., 2018) and carbon nanomaterials (Li J. et al., 2018); in addition, organic PTAs, such as small-molecule organic fluorescent dyes (Shirata et al., 2017; Gao et al., 2021), semiconducting polymers (Sun et al., 2019; Wang et al., 2019) and metal-organic frameworks (Yu et al., 2021; Liu et al., 2022; Yu et al., 2022), *etc.* For example, Chen et al. developed indocyanine green (ICG)-loaded and cancer cell membrane-coated nanoparticles (ICNPs) for homologous-targeting dual-modal imaging and photothermal therapy (Chen et al., 2016). Alves et al. explored a novel Hyaluronic acid functionalized nanoparticles loaded with IR780 and DOX which can be used for breast cancer chemo-photothermal therapy (Alves et al., 2019). Compared to the potential toxicity of inorganic PTAs, organic PTAs owned better biocompatibility and biodegradability. However, it should be noticed that the rapid metabolism and poor photostability of fluorescent dyes has limited their further applications in biomedicine. Therefore, it is necessary to modify organic PTAs with low biotoxicity, good stability and high photothermal conversion efficiency.

New indocyanine green (IR820) is a novel type of near-infrared fluorescence emissive organic dye (Jiao et al., 2020). As a derivative of indocyanine green (ICG) which is approved by the US Food and Drug Administration (FDA) (Zaharie-

Butucel et al., 2019), IR820 not only showed similar optical and photothermal properties as ICG, but also better stability and longer tissue retention (Hu et al., 2018; Meng et al., 2019; Chen et al., 2020). Given these advantages, IR820 has become an ideal organic PTA for PTT. For instance, Chen et al. used PEGylated melanin nanoparticles (PEG-MNPs) to synthesize a multifunctional theranostic agent, IR820-PEG-MNPs for *in vivo* detection and photothermal ablation of orthotopic micro-hepatocellular carcinoma (Chen et al., 2020). Jiang et al. developed an excipient-free nanodrug LA-IR820/DOX for synergetic chemo-photothermal therapy targeting hepatoma cells (Jiang et al., 2020). Xu et al. fabricated a p53 DNA/IR820 microneedle (MN) patch which co-loaded with p53 DNA and IR820 for synergistic gene therapy and PTT of subcutaneous tumor (Xu et al., 2020). However, there is little research on the simple and efficient preparation for the modification of IR820.

Polydopamine (PDA), as a kind of conjugated polymer, possesses great surface modification ability, good biocompatibility, photothermal ability and excellent photostability (Li Z. et al., 2019). More than that, PDA can be formed by a simple self-polymerization with adjustable size, and is a reliable candidate for the synthesis of PTT nanoprobe (Lv et al., 2017). These characteristics provide PDA a great potential to be a coating material as well as a photothermal material in biomedical applications (Li Z. et al., 2018; Zhang et al., 2019; Li et al., 2021).

In this work, IR820 was utilized and further encapsulated by PDA through dopamine polymerization under alkaline conditions. Then the PDA encapsulated IR820 was modified with mPEG-NH₂ via a Michael addition. The obtained IR820@PDA@PEG NPs showed a spherical morphology with an average size of 159.6 nm. And IR820@PDA@PEG NPs possessed an absorption peak at 689 nm and fluorescence peaks at 800–1,000 nm. IR820@PDA@PEG NPs exhibited good photochemical stability in different pH solutions. In addition, CCK-8 assay and photothermal experiments demonstrated the low cytotoxicity and good photothermal properties of IR820@PDA@PEG NPs, respectively. Then, IR820@PDA@PEG NPs was further utilized for the labeling of HeLa cells. Confocal microscopic images and apoptosis assay confirmed that cellular uptake ability of IR820@PDA@PEG NPs and PTT efficiency of ~49.1% under 793 nm laser irradiation. Therefore, our study demonstrated that IR820@PDA@PEG NPs could serve as a promising PTA candidate to realize PTT effect against cervical cancer HeLa cells.



SCHEME 1

Schematic illustration of the synthesis process of IR820@PDA@PEG NPs and PTT application.

Experiments

Chemicals and materials

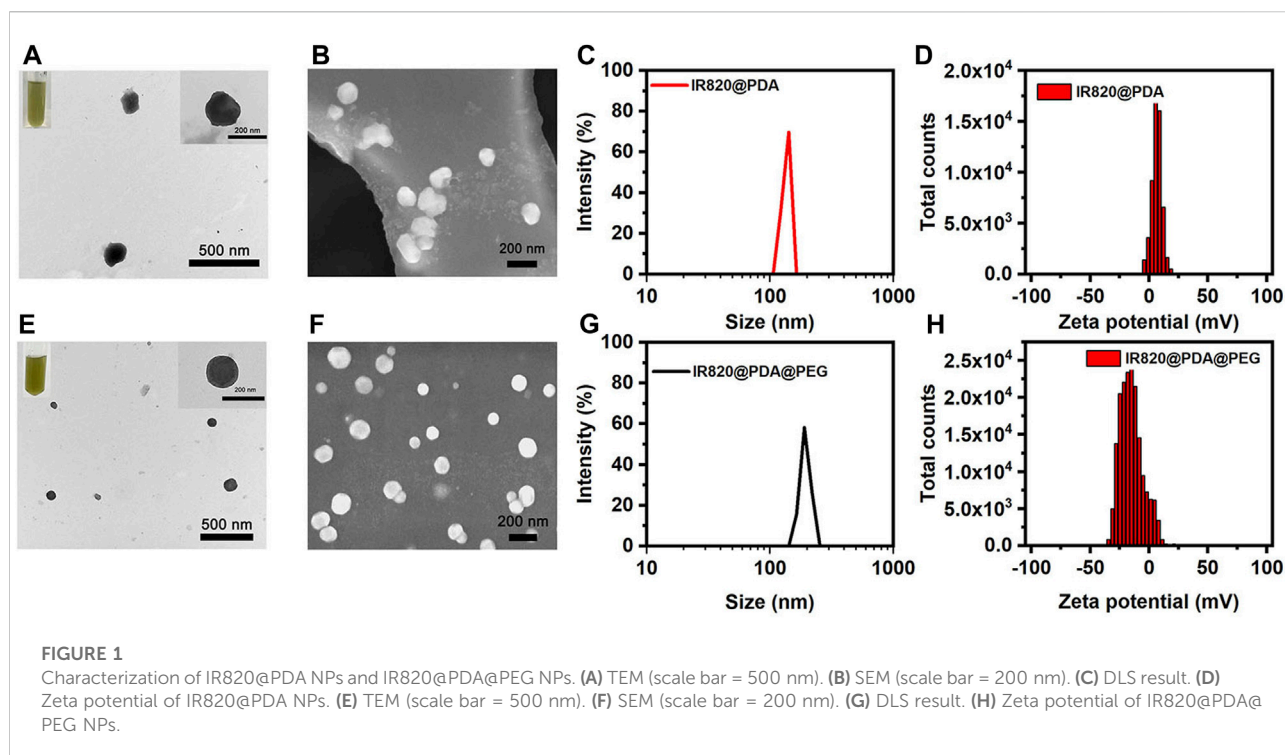
New indocyanine green (IR820, CAS:172616-80-7) was purchased from Shanghai Sigma-Aldrich (China). Dopamine (4-(2-Aminoethyl) benzene-1,2-diol, DA, CAS:51-61-6, M.W.153.18), methoxy polyethylene glycol amine (mPEG-NH₂, CAS: NONE6350, M.W. 2000) and Hoechst 33342 were obtained from Shanghai Macklin Biotechnology Co., Ltd (China). Tris-HCL buffer was received from Solarbio (Beijing, China). Phosphate buffered saline (PBS), high glucose dulbecco's modified eagle medium (DMEM) and Trypsin EDTA solution (0.25%) were all supplied by Biological Industries Israel Beit Haemek Ltd. Fetal bovine serum (FBS) was received from Shanghai Hyclone Co., Ltd (China). Cell counting kit-8 (CCK-8) was provided by Beijing Biosharp Co., Ltd. FITC Annexin V apoptosis detection kit I was supplied by BD Biosciences Pharmingen Co., Ltd (United States). All chemical reagents were used as received without further purification. Deionized (DI) water purified by a Millipore

system (New Jersey state, United States) was used in the experiments.

Preparation of IR820@PDA@PEG NPs

IR820@PDA@PEG NPs was prepared by a modified method in two steps. In the first step, 10 mg of IR820 was dissolved in 10 ml of Tris buffer solution (pH = 8.5) and sonicated for 5 min. Then, 1 mg of DA was added to the reaction vial, followed by stirring (1,200 r/min) overnight at room temperature in the dark condition. IR820@PDA NPs was purified by centrifugation (16,000 r/min, 5 min) and washed thrice with DI water.

In the second step, the obtained IR820@PDA NPs was further dissolved in 2 ml of Tris solution (pH = 8.5) and then 2 mg of mPEG-NH₂ was added. The mixture was magnetically stirred for another 24 h at room temperature in the dark condition. After that, IR820@PDA@PEG NPs was collected *via* centrifugation at 16,000 r/min for 5 min, and washed three times with DI water. The prepared IR820@PDA@PEG



NPs was dispersed in DI water and stored for subsequent evaluation.

Loading capacity (LC) and encapsulation efficiency (EE)

The LC and EE of IR820@PDA@PEG NPs were measured by a PerkinElmer UV-vis-NIR spectrometer (Lambda 750S, United States) at an absorption wavelength of 376 nm. Briefly, the absorption of free IR820 at 376 nm was measured to generate a standard curve. Then, the supernatants in two-step preparation were collected and its absorbance value was measured. Then the concentrations of IR820@PDA@PEG NPs were quantified from the standard curve. The LC and EE were calculated as follows: (Yin et al., 2020).

$$LC (\%) = \frac{\text{weight of IR820 in NPs}}{\text{total weight of NPs}} \times 100\%$$

$$EE (\%) = \frac{\text{weight of IR820 in NPs}}{\text{weight of feeding IR820}} \times 100\%$$

Characterization of IR820@PDA@PEG NPs

The morphology of IR820@PDA NPs and IR820@PDA@PEG NPs were observed by transmission electron microscopy

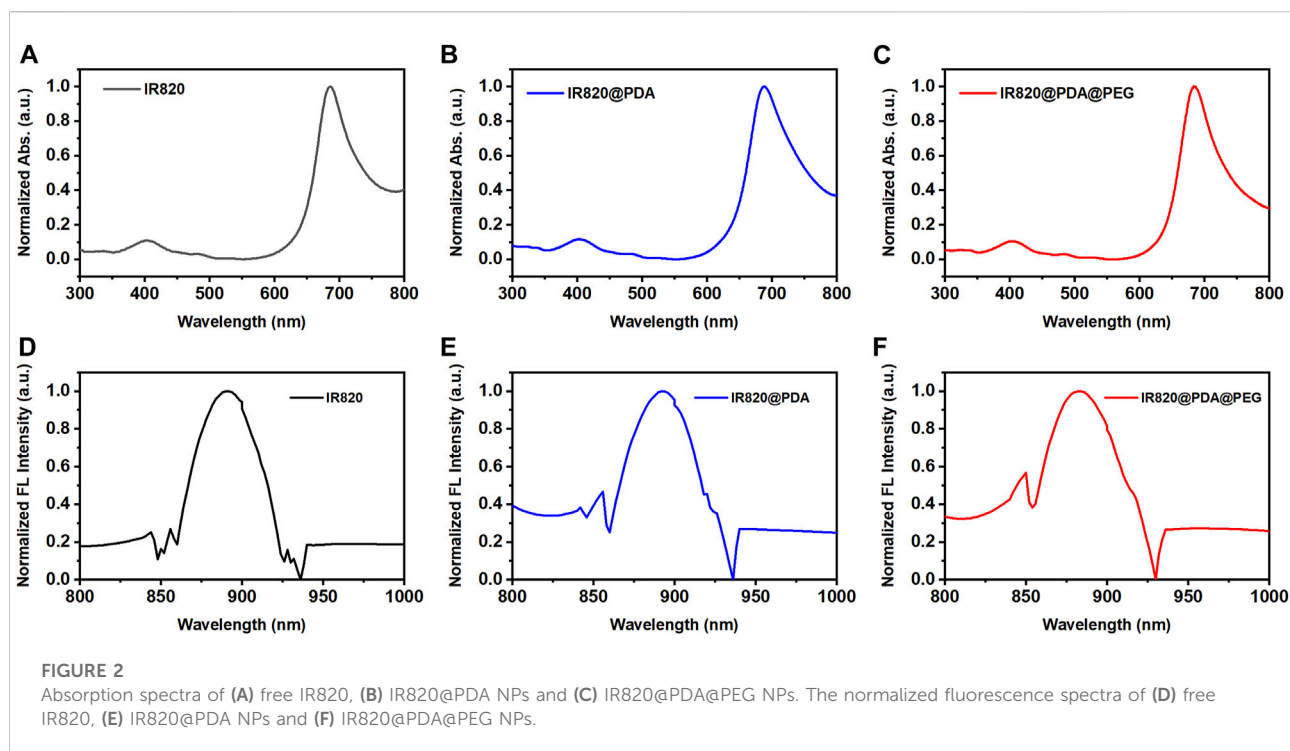
(TEM, JEM-1230, Japan). The microstructure of IR820@PDA NPs and IR820@PDA@PEG NPs were characterized by scanning electron microscopy (SEM, JSM-7610FPlus, Japan). The average size and zeta potential were measured by a Malvern Zetasizer Nano ZS-90 instrument (England). The absorption and fluorescence spectra were obtained by using a PerkinElmer UV-vis-NIR spectrometer (Lambda 750S, United States) and a Duetta fluorescence spectrometer (HORIBA, Canada), respectively. The thermal images were observed by a Fotric 323 Pro thermal camera (Shanghai Kind Electronics Co., Ltd. China).

Stability analysis

The photochemical stability of IR820@PDA@PEG NPs was evaluated as follows: IR820@PDA@PEG NPs (10 $\mu\text{g/ml}$, 4 ml) were dispersed in PBS (pH = 5.5), PBS (pH = 6.0) and PBS (pH = 7.4), respectively. The absorption spectra were monitored on a PerkinElmer UV-vis-NIR spectrometer for 1 week.

Photothermal performance of IR820@PDA@PEG NPs

To evaluate the photothermal performance of IR820@PDA@PEG NPs, same concentration of free IR820, PDA,



mNH₂-PEG and IR820@PDA@PEG NPs dispersions (100 µg/ml, 1 ml) were irradiated with 793 nm laser (300 mW/cm²) in Tris buffer, respectively. Then, the concentration-dependent temperature increase of IR820@PDA@PEG NPs were studied at different concentrations (12.5, 25, 40, 50, 80, and 100 µg/ml, 1 ml) under 793 nm laser irradiation (300 mW/cm²). Meanwhile, free IR820 (100 µg/ml) and IR820@PDA@PEG NPs (40, 80, and 100 µg/ml) were irradiated by 793 nm laser at different power densities (100, 200, 300, and 400 mW/cm²) to illustrate the dependence of temperature and power density. Moreover, after three cycles of heating and cooling, the photothermal stability was evaluated compared to free IR820.

To further assess the photothermal conversion efficiency (η), free IR820 (100 µg/ml, 1 ml) and IR820@PDA@PEG dispersions (100 µg/ml, 1 ml) were irradiated with a 793 nm laser at a power density of 300 mW/cm², respectively. When the steady-state temperature was reached, turn laser off and cool down the solutions to room temperature. The temperature variation was monitored every 30 s with a Fotric 323 Pro thermal camera. The photothermal conversion efficiency can be calculated by equation: (Zhang et al., 2018)

$$\eta (\%) = \frac{hS(T_{\max} - T_{\text{surr}})}{I(1 - 10^{-A_{793}})} \times 100\%$$

$$= \frac{m_D C_D (T_{\max} - T_{\text{surr}})}{\tau_S I (1 - 10^{-A_{793}})} \times 100\%$$

where h is the heat transfer coefficient, S is the surface area of the container. I is the laser power. m_D and C_D are the mass and the heat capacity of solvent, respectively. τ_S is the time constant. A_{793} is the absorbance of the IR820@PDA@PEG NPs at 793 nm.

Cell culture and cellular uptake

HeLa cells (a human cervical carcinoma cell line, American Type Culture Collection) were cultured in high glucose DMEM, supplemented with 10% FBS and 1% penicillin-streptomycin in a humidified incubator (37°C, 5% CO₂).

PEG NPs only group were incubated with fresh medium and IR820@PDA@PEG NPs (80 and 100 µg/ml), respectively. HeLa cells different concentrations (40, 80 and 100 µg/ml, 600 µl) in HeLa cells was investigated by confocal laser scanning microscopy (CLSM). HeLa cells were seeded into 35 mm glass-bottom dishes (1×10^5 cells per well) and incubated overnight. Then, the old medium was replaced with fresh medium containing IR820@PDA@PEG NPs. After another 2 h of incubation, HeLa cells were washed three times with $1 \times$ PBS (pH = 7.4) and counterstained with Hoechst 33342 for 5 min in the dark condition. At last, the fluorescence images of HeLa cells were detected by a Nikon fluorescence inverted microscopy (ECLIPSE-Ti, Japan).

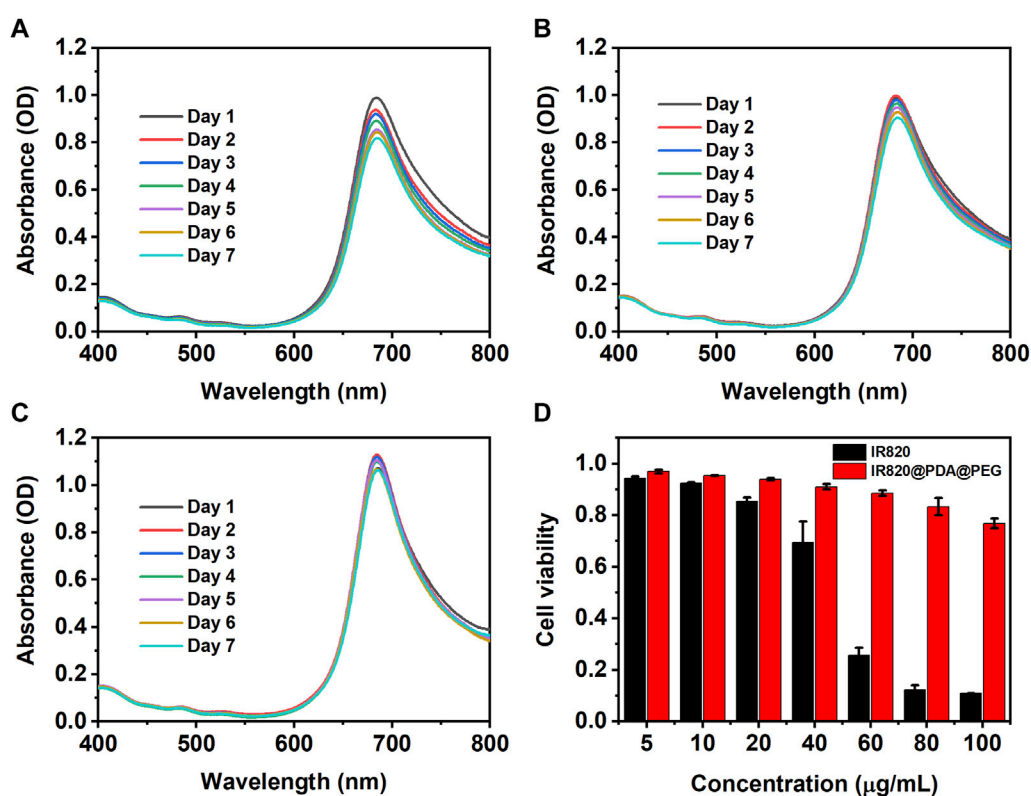


FIGURE 3

The photochemical stability of IR820@PDA@PEG NPs in pH = 5.5 (A), 6.0 (B) and 7.4. (C) aqueous solutions for 7 days (D) Cytotoxicity of HeLa cells incubated with free IR820 and IR820@PDA@PEG NPs at different concentrations (5, 10, 20, 40, 60, 80, and 100 µg/ml) for 4 h. Data are expressed as mean S.D. (n = 3 in each concentration).

In vitro cytotoxicity assay

The *in vitro* cytotoxicity assay of IR820@PDA@PEG NPs against HeLa cells was evaluated by the CCK-8 test. Briefly, HeLa cells were seeded in a 96-well plate (5×10^3 cells per well) and incubated overnight. Then, 100 µl of fresh medium with different concentrations of free IR820 and IR820@PDA@PEG NPs (5, 10, 20, 40, 60, 80, and 100 µg/ml) was added to the wells. After 4 h of incubation, CCK-8 assay was conducted according to the instructions. All experiments were performed in triplicates.

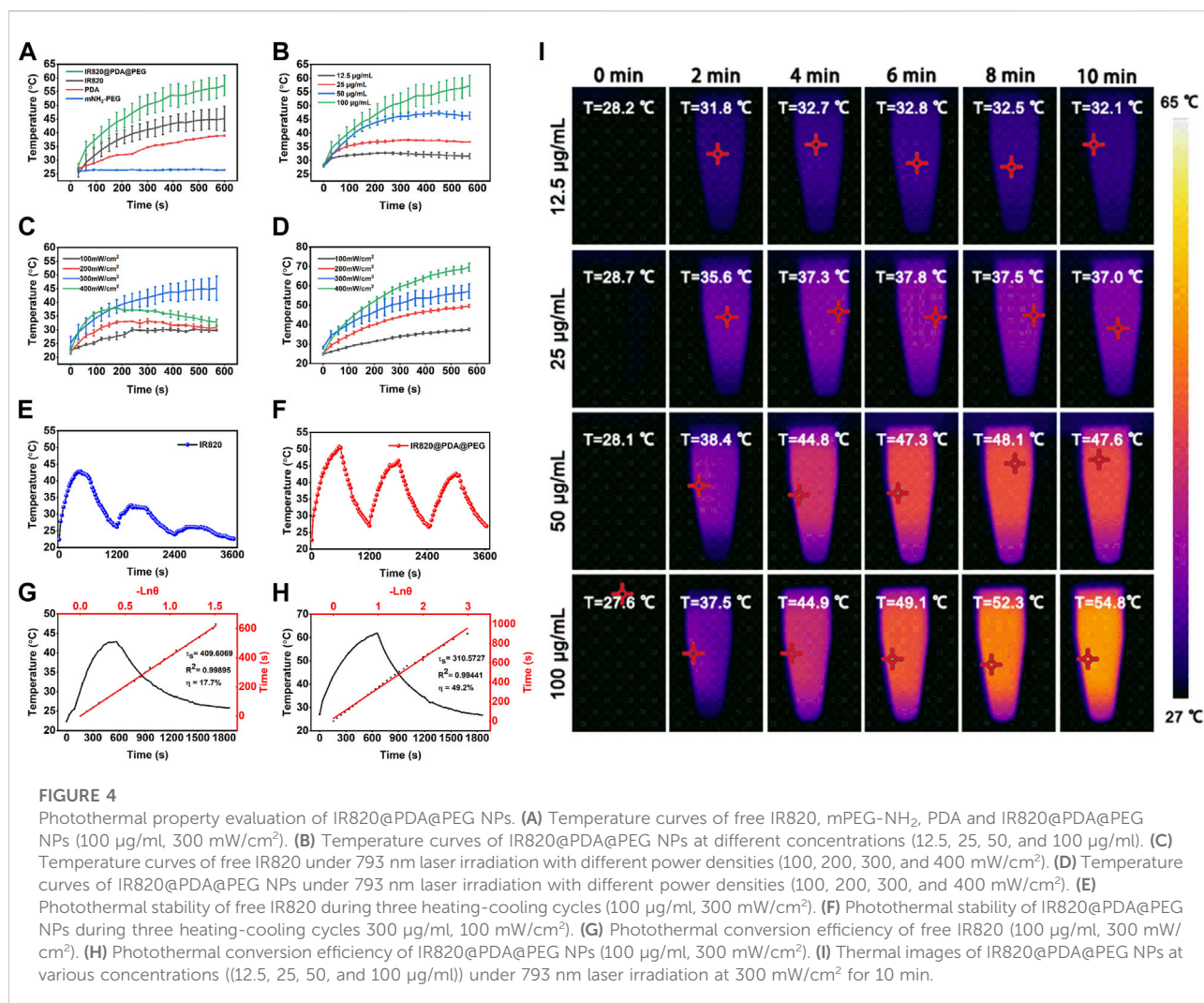
In vitro PTT evaluation

To visualize the PTT effect of IR820@PDA@PEG NPs, HeLa cells were plated in 35 mm glass-bottom cell culture dishes (1×10^5 cells per well) and cultured overnight. Afterwards, cell dishes were divided into four groups, including control group, laser only group, IR820@PDA@PEG NPs only group, and IR820@PDA@PEG NPs plus laser irradiation group.

HeLa cells in control group and IR820@PDA@PEG NPs only group were incubated with fresh medium and IR820@PDA@PEG NPs (80 and 100 µg/ml), respectively. HeLa cells in experiment group were treated with DMEM containing IR820@PDA@PEG NPs (80 and 100 µg/ml), and irradiated with a 793 nm laser (1 W/cm^2 , 8 min) simultaneously. Laser only group was treated with DMEM medium at the same laser condition. All cells were further incubated for 2 h. Then, cells were washed thrice and stained with Annexin V-FITC ($\lambda_{\text{ex}} = 488 \text{ nm}$, $\lambda_{\text{em}} = 800\text{--}1,000 \text{ nm}$) and Hoechst 33342 ($\lambda_{\text{ex}} = 488 \text{ nm}$, $\lambda_{\text{em}} = 800\text{--}1,000 \text{ nm}$) for 10 min. Finally, the CLSM images of the stained HeLa cells were acquired by a Nikon fluorescence inverted microscopy.

Apoptosis assay

To further quantify the PTT effect of IR820@PDA@PEG NPs, HeLa cells were cultured and treated with DMEM only, laser only, IR820@PDA@PEG NPs only (80 and 100 µg/ml), and IR820@PDA@PEG NPs (80 and 100 µg/ml) plus laser,



respectively. Then cells were incubated for 6 h. The groupings were consistent with PTT evaluation.

Apoptosis assay was conducted by Annexin V-FITC/PI double staining kit in strict accordance with the instructions. Briefly, HeLa cells were collected and washed three times with cold 1×PBS (pH = 7.4) softly. Then, the cells were resuspended in 100 μl of binding buffer, and co-incubated with 5 μl of Annexin V-FITC and 5 μl of PI for 10 min at room temperature in the dark condition. The cells were analyzed by a BD LSR II flow cytometer (BD Biosciences, United States) within 1 h.

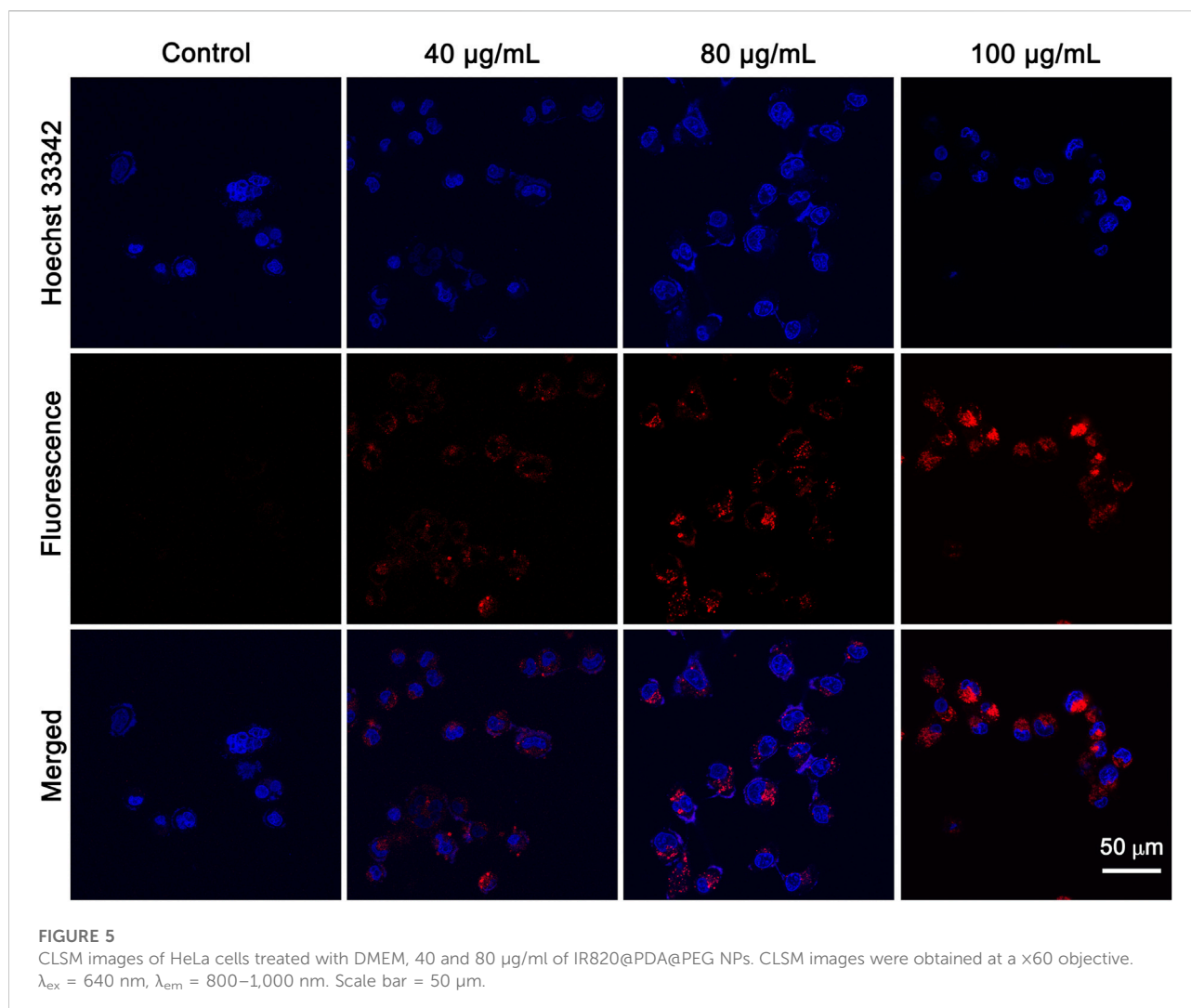
Results and discussion

Preparation and characterization of IR820@PDA@PEG NPs

In this work, IR820@PDA@PEG NPs was fabricated via a two-step surface modification (Scheme 1). Firstly, PDA

was utilized to encapsulate IR820 to enhance the biocompatibility and photothermal ability. IR820@PDA NPs was collected by centrifugation. Then, to further reduce the toxicity and improve the biocompatibility of IR820, mPEG-NH₂ was modified with IR820@PDA NPs to form IR820@PDA@PEG NPs. Then the LC and EE of IR820@PDA@PEG NPs were calculated which were 62.0 and 40.0%, respectively.

The shape of IR820@PDA NPs and IR820@PDA@PEG NPs were characterized by TEM and SEM. As shown in Figure 1A, the TEM images displayed that IR820@PDA NPs was spherical in shape, with size of approximately 129.5 nm in diameter. Figure 1B further illustrated the spherical structure of IR820@PDA NPs. Meanwhile, the color of the reaction solution changed to dark brown, indicating that PDA was successfully coated on IR820. And IR820@PDA NPs displayed a good dispersity in the aqueous solution after surface modification. Correspondingly, the TEM images as shown in Figure 1E demonstrated that IR820@PDA@PEG NPs exhibited a uniform spherical

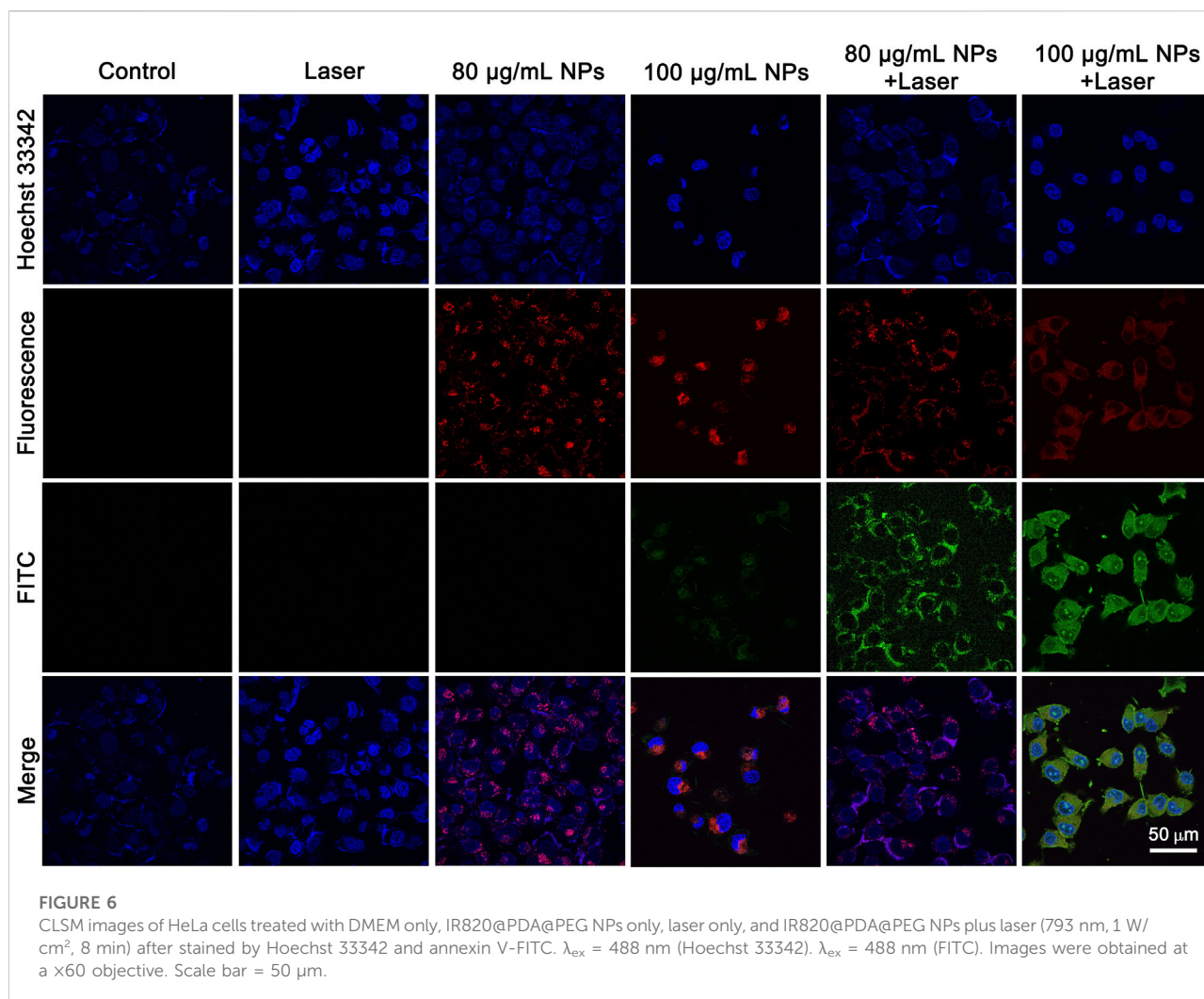


morphology with an average diameter of $\sim 159.6 \text{ nm}$. In addition, IR820@PDA@PEG NPs showed transparent brown color and good dispersion in aqueous solution. The SEM image further revealed that IR820@PDA@PEG NPs had a spherical shape (Figure 1F). As illustrated in Figures 1C, G, the average diameter of IR820@PDA NPs and IR820@PDA@PEG NPs measured by dynamic light scattering (DLS) were about 136.0, and 193.7 nm, respectively. Moreover, both IR820@PDA NPs and IR820@PDA@PEG NPs had a narrow size distribution. The increased size between two NPs demonstrated the successful coating of free IR820 with PDA, and the modification of IR820@PDA NPs with mPEG-NH₂. As illustrated in Figure 1D, the zeta potential of IR820@PDA NPs was 6.54 mV. And the zeta potential of IR820@PDA@PEG NPs decreased to -15.00 mV (Figure 1H), due to the successful modification of mPEG-NH₂. The changes of zeta potential results further confirmed that mPEG-NH₂ was assembled with IR820@PDA NPs. As shown in Supplementary Figure S1, the zeta potential changes of each

component were also measured. The zeta potentials of IR820, PDA, IR820@PDA NPs, PEG and IR820@PDA@PEG NPs were about -39.3 , -48.9 , -31.4 , -26.0 , and -15.2 mV , respectively, showing an increasing trend. These results confirmed the successful preparation of IR820@PDA NPs and IR820@PDA@PEG NPs.

Optical characterization of IR820@PDA@PEG NPs

To improve the photothermal property, biocompatibility and stability of free IR820, PDA was utilized to encapsulate IR820, and then modified with mPEG-NH₂. To investigate the optical characterization of IR820@PDA@PEG NPs, absorption spectra and fluorescence spectra of free IR820, IR820@PDA NPs, and IR820@PDA@PEG NPs were recorded, respectively. As shown in Figures 2A–C, the



absorption peak of free IR820, IR820@PDA NPs, and IR820@PDA@PEG NPs were located at 689 nm. Besides, there was no characteristic peak in the absorption spectra of DA and PEG (Supplementary Figure S2).

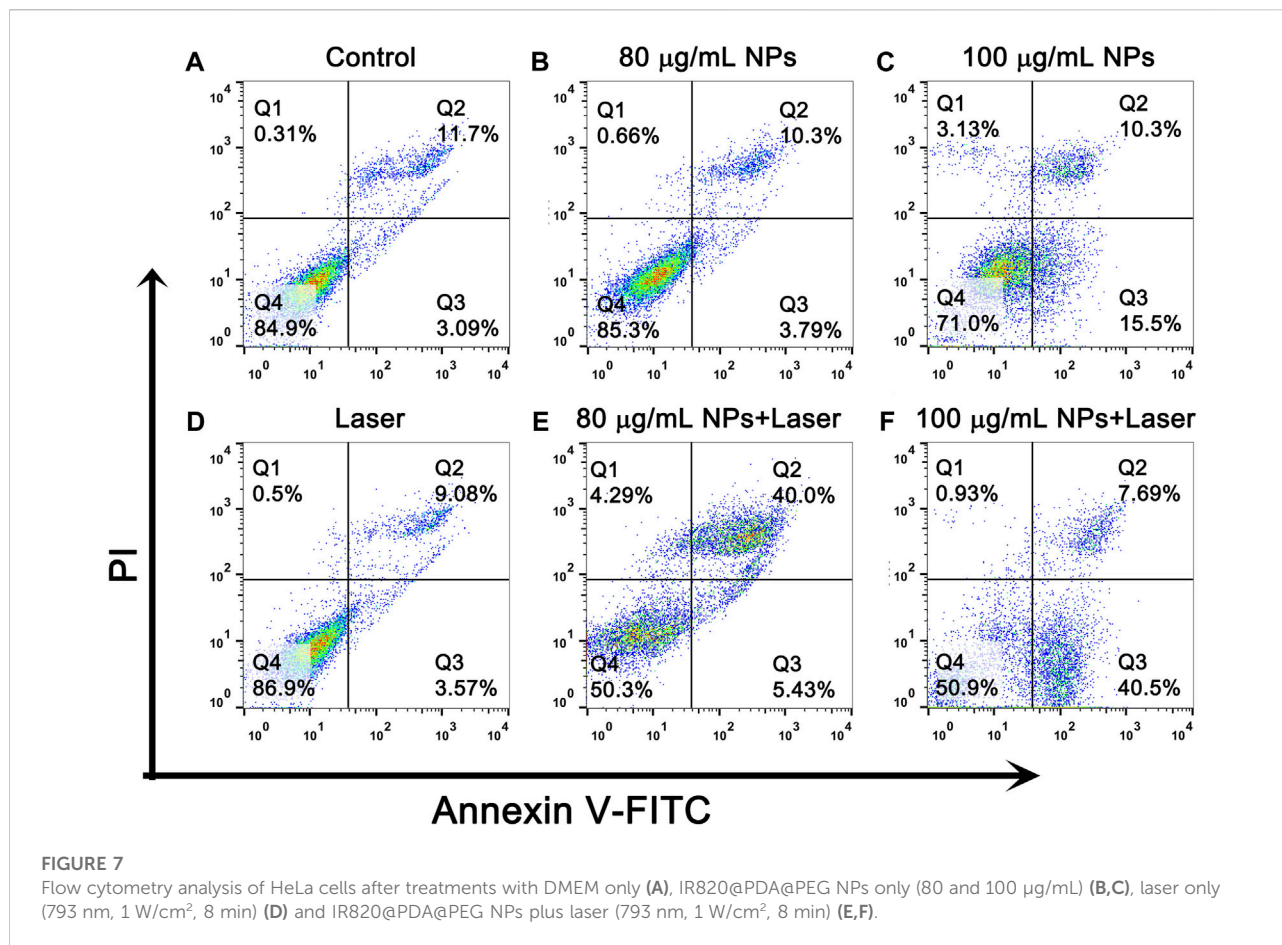
The fluorescence spectra of free IR820, IR820@PDA NPs, and IR820@PDA@PEG NPs were further measured at 450 nm excitation wavelength. The spectra are normalized with respect to the fluorescence emission peaks. As shown in Figures 2D–F, the fluorescence peak of IR820, IR820@PDA NPs, and IR820@PDA@PEG NPs were measured at a range of 800–1,000 nm. The results above showed that IR820@PDA@PEG NPs have potential in bioimaging as a NIR fluorescent probe.

Stability and CCK-8 assay

The photochemical stability of NPs is critical for their biological applications, especially for biomedical imaging

and therapy. To study the photochemical stability of IR820@PDA@PEG NPs in different pH solutions (pH = 5.5, 6.0, and 7.4), the absorption peak of IR820@PDA@PEG NPs (10 μ g/ml) was monitored for 7 days. As showed in Figures 3A–C, the shape of the spectra did not change in three different pH solutions. Compared to the absorption peak of the first day, the absorption peak of the other 6 days decreased slightly. Specifically, relative to the first day, the absorbance of the seventh day reduced from 0.99 to 0.82 (pH = 5.5), 0.99 to 0.90 (pH = 6.0), and 1.07 to 1.06 (pH = 7.4), respectively. The results indicated that IR820@PDA@PEG NPs retained well photochemical stability in various pH solutions.

Then the cytotoxicity of the obtained IR820@PDA@PEG NPs was evaluated by CCK-8 assay. As shown in Figure 3D, after 4 h incubation of HeLa cells with IR820@PDA@PEG NPs, the cell viabilities were obtained as 96.9%, 95.4%, 93.9%, 91.0%, 88.6%, 83.3%, and 76.8% at various concentrations of 5, 10, 20, 40, 60, 80, and 100 μ g/ml, respectively. In contrast, the cell



viabilities of free IR820 at the same concentrations were 92.5%, 85.4%, 69.4%, 25.7%, 12.2%, and 11.0%, respectively. The results demonstrated that IR820@PDA@PEG NPs did not cause significant cytotoxicity when the concentration was less than 100 µg/ml. Thus, IR820@PDA@PEG NPs was suitable for biomedical applications. Photothermal property evaluation of IR820@PDA@PEG NPs.

To investigate the photothermal performance of IR820@PDA@PEG NPs, the temperature rise of each component was measured. As shown in Figure 4A, under the same concentration (100 µg/ml) and laser condition (793 nm, 300 mW/cm², 10 min), the temperature change of IR820@PDA@PEG NPs was the fastest. Meanwhile, the concentration-dependent photothermal performance of IR820@PDA@PEG NPs was observed. As shown in Figure 4B, as concentrations increased, the temperature of IR820@PDA@PEG NPs raised from 28.0 to 31.6°C (12.5 µg/ml), from 28.7 to 36.8°C (25 µg/ml), from 28.2 to 46.4°C (50 µg/ml), and from 28.2 to 57.3°C (100 µg/ml), respectively. As shown in Figures 4C,D, excitation power density-dependent temperature changes of free IR820 and IR820@PDA@PEG NPs were monitored. At the optimized concentration (100 µg/ml) and excitation power density (300 mW/cm², 10 min), the

temperature rise of IR820@PDA@PEG NPs was higher than free IR820.

Then, the photothermal stability of free IR820 and IR820@PDA@PEG NPs were studied by three heat-cool cycles of laser irradiation. As illustrated in Figures 4E,F, IR820@PDA@PEG NPs exhibited better photothermal stability than free IR820. Moreover, the photothermal conversion efficiency of free IR820 and IR820@PDA@PEG NPs were observed in Figures 4G,H. The photothermal conversion efficiency (η) of IR820@PDA@PEG NPs was up to 49.2%, which was much higher than that of free IR820 (17.7%). Figure 4I was the photothermal images of IR820@PDA@PEG NPs at different concentrations, which illustrated the temperature and concentration-dependence of IR820@PDA@PEG NPs. As shown in Supplementary Figure S3, the temperature change of IR820@PDA@PEG NPs at different concentrations (40 and 80 µg/ml) under different power densities (100, 200, 300, and 400 mW/cm²) further illustrated the concentration and power dependence photothermal property of IR820@PDA@PEG NPs. These results indicated that IR820@PDA@PEG NPs owned enhanced photothermal performance and photothermal

stability than free IR820. These results demonstrated that IR820@PDA@PEG NPs showed excellent photothermal performance, which laid a good foundation for further PTT studies of HeLa cells.

Cellular uptake

Effective cellular uptake of NPs is the prerequisite for efficient cancer therapy. CLSM was performed to investigate the cellular uptake ability of IR820@PDA@PEG NPs in HeLa cells. The nucleus and cytoplasm were stained with Hoechst 33342 (blue channel) and IR820@PDA@PEG NPs (red channel). HeLa cells were incubated with DMEM, 40, 80, and 100 $\mu\text{g/ml}$ of IR820@PDA@PEG NPs for 2 h, respectively. As shown in Figure 5, HeLa cells treated with IR820@PDA@PEG NPs showed fluorescence signals in red channel, which demonstrated that IR820@PDA@PEG NPs can be effectively internalized by HeLa cells and was predominately presented in the cytoplasm. Besides, the fluorescence intensity in red channel with 100 $\mu\text{g/ml}$ of IR820@PDA@PEG NPs group was brighter than that of 40 and 80 $\mu\text{g/ml}$, indicating that the cellular uptake of IR820@PDA@PEG NPs exhibited a concentration-dependent property. The results above illustrated that IR820@PDA@PEG NPs can be efficiently taken up by HeLa cells.

In vitro PTT effect of IR820@PDA@PEG NPs

The PTT effect of IR820@PDA@PEG NPs on HeLa cells was analyzed by Annexin V-FITC and Hoechst 33342 staining. It is well known that cells stained with Hoechst 33342 is to visualize nucleus (blue channel) and Annexin V-FITC is to detect apoptotic cells (green channel). As shown in Figure 6, cells treated by either DMEM only or laser only exhibited fluorescence signals in blue channel, which indicated the harmlessness of 793 nm laser only (1 W/cm², 8 min) to HeLa cells. And the CLSM images in IR820@PDA@PEG NPs (80 $\mu\text{g/ml}$) only group showed fluorescence signals in blue and red channels, which indicated that IR820@PDA@PEG NPs was entered into cells and owned biocompatibility. Moreover, apoptosis occurred in cells treated with IR820@PDA@PEG NPs (100 $\mu\text{g/ml}$) only. HeLa cells in IR820@PDA@PEG NPs (80 and 100 $\mu\text{g/ml}$) plus laser group showed fluorescence signals in blue, red, and green channels, verifying that IR820@PDA@PEG NPs induced apoptosis under 793 nm laser irradiation (1 W/cm², 8 min). Besides, more apparently apoptotic cells were observed in 100 $\mu\text{g/ml}$ of IR820@PDA@PEG NPs plus laser group compared to that of 80 $\mu\text{g/ml}$ (fluorescence signals in green channel).

To further quantitatively confirm the *in vitro* PTT effect of IR820@PDA@PEG NPs, cell apoptosis and necrosis were detected by apoptosis assay. As shown in Figures 7A–D, the percentage of cell death in control group, laser only group, 80 and 100 $\mu\text{g/ml}$

IR820@PDA@PEG NPs group were 15.1%, 13.1%, 14.8% and 29.0%, respectively. However, the death ratio in 80 and 100 $\mu\text{g/ml}$ IR820@PDA@PEG NPs plus laser group was remarkably improved to 49.7% and 49.1% (Figures 7E,F). Therefore, IR820@PDA@PEG NPs had the photothermal cytotoxicity against HeLa cells under 793 nm laser irradiation. Moreover, HeLa cells incubated with IR820@PDA@PEG NPs showed massive apoptosis, demonstrating their hopeful application in the photothermal treatment of cervical cancer HeLa cells.

Conclusion

In summary, a novel type of IR820@PDA@PEG NPs was designed and synthesized *via* a two-step surface modification. IR820@PDA@PEG NPs showed low cytotoxicity, improved biocompatibility, and super photochemical stability. In addition, IR820@PDA@PEG NPs possessed excellent photothermal performance and substantially improved photothermal conversion efficiency about 49.2% under 793 nm laser irradiation. Moreover, confocal microscopic images showed the concentration-dependent cellular labeling ability of IR820@PDA@PEG NPs. Annexin V-FITC and Hoechst 33342 staining revealed the excellent PTT of IR820@PDA@PEG NPs under 793 nm laser irradiation. The flow cytometry results further indicated the growth of HeLa cells could be effectively inhibited with the assistance of IR820@PDA@PEG NPs under 793 nm laser irradiation. Taken together, as a kind of biocompatible biomaterial, IR820@PDA@PEG NPs has a great potential for PTT against cervical cancer HeLa cells.

Data availability statement

The original contributions presented in the study are included in the article/Supplementary Material, further inquiries can be directed to the corresponding authors.

Author contributions

Conceptualization: NA, XZ, HF, and ZD; methodology: HF, TY, SC, XT, and YH; data curation: HF and TY; analysis and investigation: GA and LZ, and RM; writing—original draft: HF; writing—review: NA, XZ, and HF; All authors contributed to the article and approved the submitted version.

Funding

This work was financially supported by Natural Science Foundation of Xinjiang Uygur Autonomous Region (2022D01C213 and 2020D01C151), National Natural Science

Foundation of China (82060326 and 62035011), Xinjiang Medical University/State Key Laboratory of Pathogenesis, Prevention and Treatment of High Incidence Diseases in Central cultivation project of National Science Foundation for outstanding young people (xyd2021Y005), and Fundamental Research Funds for the Central Universities and State Key Laboratory of Pathogenesis, Prevention and Treatment of High Incidence Diseases in Central Asia Fund (SKL-HIDCA-2022-3 and SKL-HIDCA-2022-GJ1).

Conflict of interest

The authors declare that the research was conducted in the absence of any commercial or financial relationships that could be construed as a potential conflict of interest.

References

- Alves, C. G., de Melo-Diogo, D., Lima-Sousa, R., Costa, E. C., and Correia, I. J. (2019). Hyaluronic acid functionalized nanoparticles loaded with IR780 and DOX for cancer chemo-photothermal therapy. *Eur. J. Pharm. Biopharm.* 137, 86–94. doi:10.1016/j.ejpb.2019.02.016
- Chen, J., Ning, C., Zhou, Z., Yu, P., Zhu, Y., Tan, G., et al. (2019). Nanomaterials as photothermal therapeutic agents. *Prog. Mat. Sci.* 99, 1–26. doi:10.1016/j.pmatsci.2018.07.005
- Chen, K., Li, Q., Zhao, X., Zhang, J., Ma, H., Sun, X., et al. (2020). Biocompatible melanin based theranostic agent for *in vivo* detection and ablation of orthotopic micro-hepatocellular carcinoma. *Biomater. Sci.* 8 (15), 4322–4333. doi:10.1039/d0bm00825g
- Chen, Z., Zhao, P., Luo, Z., Zheng, M., Tian, H., Gong, P., et al. (2016). Cancer cell membrane-biomimetic nanoparticles for homologous-targeting dual-modal imaging and photothermal therapy. *ACS Nano* 10 (11), 10049–10057. doi:10.1021/acsnano.6b04695
- Cohen, P. A., Jhingran, A., Oaknin, A., and Denny, L. (2019). Cervical cancer. *Lancet* 393 (10167), 169–182. doi:10.1016/s0140-6736(18)32470-x
- Dong, X., Liang, J., Yang, A., Qian, Z., Kong, D., and Lv, F. (2019). Fluorescence imaging guided CpG nanoparticles-loaded IR820-hydrogel for synergistic photothermal immunotherapy. *Biomaterials* 209, 111–125. doi:10.1016/j.biomaterials.2019.04.024
- Enokida, T., Moreira, A., and Bhardwaj, N. (2021). Vaccines for immunoprevention of cancer. *J. Clin. Invest.* 131 (9), 146956. doi:10.1172/jci146956
- Gao, Z., Li, C., Shen, J., and Ding, D. (2021). Organic optical agents for image-guided combined cancer therapy. *Biomed. Mat.* 16 (4), 042009. doi:10.1088/1748-605X/abf980
- Ginsburg, O., Badwe, R., Boyle, P., Derricks, G., Dare, A., Evans, T., et al. (2017). Changing global policy to deliver safe, equitable, and affordable care for women's cancers. *Lancet* 389 (10071), 871–880. doi:10.1016/s0140-6736(16)31393-9
- Hong, S., Zheng, D. W., Zhang, C., Huang, Q. X., Cheng, S. X., and Zhang, X. Z. (2020). Vascular disrupting agent induced aggregation of gold nanoparticles for photothermally enhanced tumor vascular disruption. *Sci. Adv.* 6 (23), eabb0020. doi:10.1126/sciadv.abb0020
- Hu, K., Xie, L., Zhang, Y., Hanyu, M., Yang, Z., Nagatsu, K., et al. (2020). Marriage of black phosphorus and Cu(2+) as effective photothermal agents for PET-guided combination cancer therapy. *Nat. Commun.* 11 (1), 2778. doi:10.1038/s41467-020-16513-0
- Hu, X., Tian, H., Jiang, W., Song, A., Li, Z., and Luan, Y. (2018). Rational design of IR820- and Ce6-based versatile micelle for single NIR laser-induced imaging and dual-modal phototherapy. *Small* 14 (52), e1802994. doi:10.1002/smll.201802994
- Jiang, Y., Huang, C., and Luan, Y. (2020). Lactosylated IR820/DOX co-assembled nanodrug for synergistic antitumor therapy. *Int. J. Nanomedicine* 15, 4431–4440. doi:10.2147/IJN.S247617

Publisher's note

All claims expressed in this article are solely those of the authors and do not necessarily represent those of their affiliated organizations, or those of the publisher, the editors and the reviewers. Any product that may be evaluated in this article, or claim that may be made by its manufacturer, is not guaranteed or endorsed by the publisher.

Supplementary material

The Supplementary Material for this article can be found online at: <https://www.frontiersin.org/articles/10.3389/fbioe.2022.984166/full#supplementary-material>

- Jiao, L., Liu, Y., Zhang, X., Hong, G., Zheng, J., Cui, J., et al. (2020). Constructing a local hydrophobic cage in dye-doped fluorescent silica nanoparticles to enhance the photophysical properties. *ACS Cent. Sci.* 6 (5), 747–759. doi:10.1021/acscentsci.0c00071
- Li, J., Liu, X., Tan, L., Cui, Z., Yang, X., Liang, Y., et al. (2019a). Zinc-doped Prussian blue enhances photothermal clearance of *Staphylococcus aureus* and promotes tissue repair in infected wounds. *Nat. Commun.* 10 (1), 4490. doi:10.1038/s41467-019-12429-6
- Li, J., Zhang, Z., Deng, H., and Zheng, Z. (2021). Cinobufagin-loaded and folic acid-modified polydopamine nanomedicine combined with photothermal therapy for the treatment of lung cancer. *Front. Chem.* 9, 637754. doi:10.3389/fchem.2021.637754
- Li, J., Zu, X., Liang, G., Zhang, K., Liu, Y., Li, K., et al. (2018a). Octopod PtCu nanoframe for dual-modal imaging-guided synergistic photothermal radiotherapy. *Theranostics* 8 (4), 1042–1058. doi:10.7150/thno.22557
- Li, Z., Chen, Y., Yang, Y., Yu, Y., Zhang, Y., Zhu, D., et al. (2019b). Recent advances in nanomaterials-based chemo-photothermal combination therapy for improving cancer treatment. *Front. Bioeng. Biotechnol.* 7, 293. doi:10.3389/fbioe.2019.00293
- Li, Z., Wang, B., Zhang, Z., Wang, B., Xu, Q., Mao, W., et al. (2018b). Radionuclide imaging-guided chemo-radioisotope synergistic therapy using a 131I-labeled polydopamine multifunctional nanocarrier. *Mol. Ther.* 26 (5), 1385–1393. doi:10.1016/j.yimthe.2018.02.019
- Liu, S., Wen, M., Huang, M., Wang, H., Chen, Z., and Yu, N. (2022). Nanoscale hematoporphrin-based frameworks for photo-sono synergistic cancer therapy via utilizing Al(III) as metal nodes rather than heavy metals. *J. Colloid Interface Sci.* 616, 23–33. doi:10.1016/j.jcis.2022.02.040
- Liu, Y., Wang, H., Li, S., Chen, C., Xu, L., Huang, P., et al. (2020). *In situ* supramolecular polymerization-enhanced self-assembly of polymer vesicles for highly efficient photothermal therapy. *Nat. Commun.* 11 (1), 1724. doi:10.1038/s41467-020-15427-1
- Lungu, I., Grumezescu, A. M., Volceanov, A., and Andronescu, E. (2019). Nanobiomaterials used in cancer therapy: An up-to-date overview. *Molecules* 24 (19), 3547. doi:10.3390/molecules24193547
- Lv, R., Yang, P., Chen, G., Gai, S., Xu, J., and Prasad, P. N. (2017). Dopamine-mediated photothermal theranostics combined with up-conversion platform under near infrared light. *Sci. Rep.* 7 (1), 13562. doi:10.1038/s41598-017-13284-5
- Meng, X., Wang, K., Lv, L., Zhao, Y., Sun, C., Ma, L., et al. (2019). Photothermal/Photodynamic therapy with immune-adjunct liposomal complexes for effective gastric cancer therapy. *Part. Part. Syst. Character.* 36 (6), 1900015. doi:10.1002/ppsc.201900015
- Meng, Z., Wei, F., Wang, R., Xia, M., Chen, Z., Wang, H., et al. (2016). NIR-laser-switched *in vivo* smart nanocapsules for synergic photothermal and chemotherapy of tumors. *Adv. Mat.* 28 (2), 245–253. doi:10.1002/adma.201502669
- Nam, J., Son, S., Ochyl, L. J., Kuai, R., Schwendeman, A., and Moon, J. J. (2018). Chemo-photothermal therapy combination elicits anti-tumor immunity against advanced metastatic cancer. *Nat. Commun.* 9 (1), 1074. doi:10.1038/s41467-018-03473-9

- Nuo, W., Zhaojie, Z., Jiulong, L., Liu, Z., Zhu, B., Yu, J., et al. (2018). Thiol-capped Bi nanoparticles as stable and all-in-one type theranostic nanoagents for tumor imaging and thermoradiotherapy. *Biomaterials* 161, 279–291. doi:10.1016/j.biomaterials.2018.01.047
- Ren, D., Hua, Y., Yu, B., Ye, X., He, Z., Li, C., et al. (2020). Predictive biomarkers and mechanisms underlying resistance to PD1/PD-L1 blockade cancer immunotherapy. *Mol. Cancer* 19 (1), 19. doi:10.1186/s12943-020-1144-6
- Schiffman, M., Doorbar, J., Wentzensen, N., de Sanjosé, S., Fakhry, C., Monk, B. J., et al. (2016). Carcinogenic human papillomavirus infection. *Nat. Rev. Dis. Prim.* 2, 16086. doi:10.1038/nrdp.2016.86
- Shirata, C., Kaneko, J., Inagaki, Y., Kokudo, T., Sato, M., Kiritani, S., et al. (2017). Near-infrared photothermal/photodynamic therapy with indocyanine green induces apoptosis of hepatocellular carcinoma cells through oxidative stress. *Sci. Rep.* 7 (1), 13958. doi:10.1038/s41598-017-14401-0
- Sun, T., Han, J., Liu, S., Wang, X., Wang, Z. Y., and Xie, Z. (2019). Tailor-made semiconducting polymers for second near-infrared photothermal therapy of orthotopic liver cancer. *ACS Nano* 13 (6), 7345–7354. doi:10.1021/acsnano.9b03910
- Wang, S., Zhang, L., Zhao, J., He, M., Huang, Y., and Zhao, S. (2021). A tumor microenvironment-induced absorption red-shifted polymer nanoparticle for simultaneously activated photoacoustic imaging and photothermal therapy. *Sci. Adv.* 7 (12), eabe3588. doi:10.1126/sciadv.abe3588
- Wang, X., Geng, Z., Cong, H., Shen, Y., and Yu, B. (2019). Organic semiconductors for photothermal therapy and photoacoustic imaging. *ChemBiochem* 20 (13), 1628–1636. doi:10.1002/cbic.201800818
- Wang, Z., Yu, N., Li, X., Yu, W., Han, S., Ren, X., et al. (2020a). Galvanic exchange-induced growth of Au nanocrystals on CuS nanoplates for imaging guided photothermal ablation of tumors. *Chem. Eng. J.* 381, 122613. doi:10.1016/j.cej.2019.122613
- Wang, Z., Yu, W., Yu, N., Li, X., Feng, Y., Geng, P., et al. (2020b). Construction of CuS@Fe-MOF nanoplateforms for MRI-guided synergistic photothermal-chemo therapy of tumors. *Chem. Eng. J.* 400, 125877. doi:10.1016/j.cej.2020.125877
- Xiao, C., Tong, C., Fan, J., Wang, Z., Xie, Q., Long, Y., et al. (2021). Biomimetic nanoparticles loading with gamabutin-indomethacin for chemo/photothermal therapy of cervical cancer and anti-inflammation. *J. Control. Release* 339, 259–273. doi:10.1016/j.jconrel.2021.09.034
- Xu, Q., Li, X., Zhang, P., and Wang, Y. (2020). Rapidly dissolving microneedle patch for synergistic gene and photothermal therapy of subcutaneous tumor. *J. Mat. Chem. B* 8 (19), 4331–4339. doi:10.1039/d0tb00105h
- Yin, W., Zhao, Y., Kang, X., Zhao, P., Fu, X., Mo, X., et al. (2020). BBB-penetrating codelivery liposomes treat brain metastasis of non-small cell lung cancer with EGFR(T790M) mutation. *Theranostics* 10 (14), 6122–6135. doi:10.7150/thno.42234
- Yu, N., Hu, Y., Wang, X., Liu, G., Wang, Z., Liu, Z., et al. (2017). Dynamically tuning near-infrared-induced photothermal performances of TiO₂ nanocrystals by nb-doping for imaging guided photothermal therapy of tumors. *Nanoscale* 9, 9148–9159. doi:10.1039/c7nr02180a
- Yu, N., Li, J., Wang, Z., Yang, S., Liu, Z., Wang, Y., et al. (2018). Blue Te nanoneedles with strong NIR photothermal and laser-enhanced anticancer effects as "All-in-One" nanoagents for synergistic thermo-chemotherapy of tumors. *Adv. Healthc. Mat.* 7 (21), e1800643. doi:10.1002/adhm.201800643
- Yu, N., Qiu, P., Ren, Q., Wen, M., Geng, P., Macharia, D. K., et al. (2021). Transforming a sword into a knife: Persistent phototoxicity inhibition and alternative therapeutical activation of highly-photosensitive phytochlorin. *ACS Nano* 15 (12), 19793–19805. doi:10.1021/acsnano.1c07241
- Yu, N., Tu, W., Qiu, P., Ren, Q., Chen, X., Zhu, M., et al. (2022). Full-route advances via biomimetic and biodegradable ultrasmall-in-nano architectures with radiation-photo synergy. *Nano Today* 43, 101427. doi:10.1016/j.nantod.2022.101427
- Zaharie-Butucel, D., Potara, M., Suarasan, S., Licarete, E., and Astilean, S. (2019). Efficient combined near-infrared-triggered therapy: Phototherapy over chemotherapy in chitosan-reduced graphene oxide-IR820 dye-doxorubicin nanoplateforms. *J. Colloid Interface Sci.* 552, 218–229. doi:10.1016/j.jcis.2019.05.050
- Zhang, D., Zhang, J., Li, Q., Tian, H., Zhang, N., Li, Z., et al. (2018). pH- and enzyme-sensitive IR820-paclitaxel conjugate self-assembled nanovehicles for near-infrared fluorescence imaging-guided chemo-photothermal therapy. *ACS Appl. Mat. Interfaces* 10 (36), 30092–30102. doi:10.1021/acscami.8b09098
- Zhang, J., Fan, J., Skwarczynski, M., Stephenson, R. J., Toth, I., and Hussein, W. M. (2022). Peptide-based nanovaccines in the treatment of cervical cancer: A review of recent advances. *Int. J. Nanomedicine* 17, 869–900. doi:10.2147/ijn.S269986
- Zhang, Y., Xiu, W., Gan, S., Shan, J., Ren, S., Yuwen, L., et al. (2019). Antibody-functionalized MoS₂ nanosheets for targeted photothermal therapy of staphylococcus aureus focal infection. *Front. Bioeng. Biotechnol.* 7, 218. doi:10.3389/fbioe.2019.00218